Isotope fractionation induced by phase transformation: First-principles investigation for Mg_2SiO_4

Zhongqing Wu [a,b,*], Fang Huang [c], Shichun Huang [d]

[a] Laboratory of Seismology and Physics of Earth's Interior, School of Earth and Space Sciences, University of Science and Technology of China, Hefei, Anhui 230026, China
[b] Mengcheng National Geophysical Observatory, Anhui, China
[c] CAS Key Laboratory of Crust-Mantle Materials and Environments, School of Earth and Space Sciences, University of Science and Technology of China, Hefei, Anhui 230026, China
[d] Department of Geoscience, University of Nevada, Las Vegas, NV 89154, United States

A B S T R A C T

With increasing pressure, olivine transforms to wadsleyite, ringwoodite, and finally dissociates into bridgmanite and ferropericlase, producing dramatic structure changes along these phase transformations. Here we investigated the equilibrium isotope fractionation of Mg, Si, and O among these phases using first-principles calculations. Both Mg and Si have measurable isotope fractionations among these phases, even at mantle's pressure–temperature conditions. Wadsleyite and ringwoodite are depleted in heavy Si but enriched in heavy Mg relative to olivine. Bridgmanite is depleted in heavy Si and Mg among all phases. Increasing pressure can slightly reduce the size of Si isotope fractionation but significantly depress Mg isotope fractionation among these phases. Mg and Si isotope fractionation among Mg_2SiO_4 polymorphs may provide a promising way to "probe" the depth and temperature of origin of mantle xenoliths.

© 2014 Elsevier B.V. All rights reserved.

1. Introduction

Inter-mineral isotope fractionations are important in estimating temperatures for many geological processes (e.g. Anderson et al., 1971; Clayton, 1986; Emiliani, 1955; Valley, 2001) and elucidating the material fluxes and time scales associated with magmatism and fluid/melt–rock interaction in the crust and mantle (see Valley, 1986; Zheng et al., 2003). Equilibrium isotope fractionation factors are the bases for the interpretation of isotope fractionation data from natural systems, and they are essential geochemical parameters in evaluating isotopic equilibrium (e.g. Chakrabarti and Jacobsen, 2010b; Feng et al., 2014; Huang et al., 2013; Schauble, 2011; Teng et al., 2011; Young et al., 2009).

The equilibrium fractionation of stable isotopes was thought to be negligible at the mantle's temperature (T) and pressure (P) conditions because isotope fractionation is proportional to $1/T^2$ (Urey, 1947). With the advent of modern analytical techniques such as multi-collector inductively-coupled plasma mass spectrometry (MC-ICP-MS) (e.g. Albarede and Beard, 2004), inter-mineral

Mg isotope fractionation has been observed among mafic minerals even at mantle P–T conditions because of their structural differences (Bourdon et al., 2010; Chakrabarti and Jacobsen, 2010a; Handler et al., 2009; Huang et al., 2009; Li et al., 2011; Liu et al., 2011; Teng et al., 2007, 2010; Tipper et al., 2008a, 2008b; Wang et al., 2012; Wiechert and Halliday, 2007; Young and Galy, 2004; Young et al., 2002, 2009). Equilibrium isotope fractionation is sensitive to the bond strength with the heavier isotopes preferring the stronger bond. Phase transformations in the Earth's deep interior change the bond strengths of many minerals, which may produce measurable effects on equilibrium isotope fractionations. These isotope fractionations, if confirmed in natural samples or by laboratory experiments, will provide a potential way to estimate the depth of origin of these natural samples.

Olivine is the most abundant mineral in the upper mantle. With increasing pressure, olivine transforms to wadsleyite, then to ringwoodite, and finally dissociates into bridgmanite and ferropericlase (Ito and Takahashi, 1989; Katsura and Ito, 1989; Liu, 1976; Ringwood, 1991). The global seismic discontinuities at ~410 km and 670 km and local seismic discontinuity at ~520 km have been ascribed to these transformations. The remarkable changes on the lattice structure and vibrational properties (see Li et al., 2007; Wu and Wentzcovitch, 2007; Yu and Wentzcovitch, 2006; Yu et al., 2008) caused by these transformations may significantly

impact the equilibrium Mg, Si, and O isotope fractionations among these phases.

Following the pioneering work by Kieffer (1982), recent studies have demonstrated that the first-principles calculation based on density functional theory is a powerful tool for calculating equilibrium fractionation factors of stable isotopes (e.g. Blanchard et al., 2009; Feng et al., 2014; Huang et al., 2013, 2014; Javoy et al., 2012; Li and Liu, 2011; Li et al., 2009; Meheut et al., 2007, 2009; Rustad and Dixon, 2009; Rustad and Yin, 2009; Schauble, 2004, 2011). In this study, we use this approach to investigate the equilibrium fractionations of Mg_2SiO_4 (olivine, its polymorphs, bridgmanite, and ferropericlase) for Mg, Si, and O isotopes. These fractionation factors are important in determining whether isotope fractionations in natural samples, such as mantle xenolith and inclusions in diamonds, are caused by phase transformations and hence potentially provide a way to trace the depth of the origin of these natural samples. This approach is complementary to other ways of estimating the depth of origin of the xenoliths based on major element compositions, such as mineral reactions and geobarometric methods (e.g. Collerson et al., 2000; Harte, 2010; Kaminsky et al., 2001; Keshav and Sen, 2001; Pearson et al., 2014).

2. Calculation details

The dependence of the vibrational frequencies on isotopic mass on a particular bond leads to isotope fractionation (Bigeleisen and Mayer, 1947; Kieffer, 1982; Urey, 1947). The equilibrium isotope fractionation factor of element X between phases A and B is defined as the ratio of their isotope ratios in these two phases and given as $\alpha_{A-B} = \beta_A / \beta_B$, where β is the reduced partition function ratio. In the harmonic approximation β is:

$$\beta = \left(\frac{Q^*}{Q} \right) = \prod_i^{3N} \frac{u_i^*}{u_i} \frac{e^{-\frac{1}{2}u_i^*}}{(1-e^{-u_i^*})} \frac{(1-e^{-u_i})}{e^{-\frac{1}{2}u_i}}, \tag{1}$$

where Q is the vibrational partition function, asterisk refers to the heavy isotope, $u_i = \hbar\omega_i/K_BT$, ω_i is the vibrational frequency of mode i, K_B and $\hbar$ are the Boltzmann and Planck constants, respectively, T is the temperature in Kelvin, and N is the number of atoms in the unit cell.

β is a function of the unit cell volume, pressure and temperature. Equation of state, $P(V,T) = -\partial F(V,T)/\partial T$, is needed to express β as a function of P and T. Helmholtz free energy $F(V,T)$ in the quasi-harmonic approximation is given by:

$$F(V,T) = U(V) + \sum_{qj} \frac{\hbar\omega_{qj}(V)}{2} + K_BT \sum_{qj} \ln\left(1 - \exp\left[\frac{\hbar\omega_{qj}(V)}{K_B} \right] \right) \tag{2}$$

where q is the wave vector in the first Brillouin zone, j is the index of phonon mode with frequency ω_{qj}. The first, second, and third terms in Eq. (2) are the static internal, zero-point, and vibrational energy contributions, respectively. The calculated Helmholtz free energy versus volume is fitted by the third-order Birch–Murnaghan finite strain equation of states to obtain the $P(V,T)$. The quasi-harmonic approximation has been demonstrated to work well for many minerals (Wentzcovitch et al., 2010; Wu, 2010; Wu and Wentzcovitch, 2011).

Electric structures and vibrational frequencies of minerals are calculated using Quantum espresso, a package based on density functional theory, plane wave, and pseudopotential (Giannozzi et al., 2009). The calculation details for minerals discussed in this study are similar to previous studies with the same pseudopotential for Mg, Si, and O (Huang et al., 2013; Karki et al.,
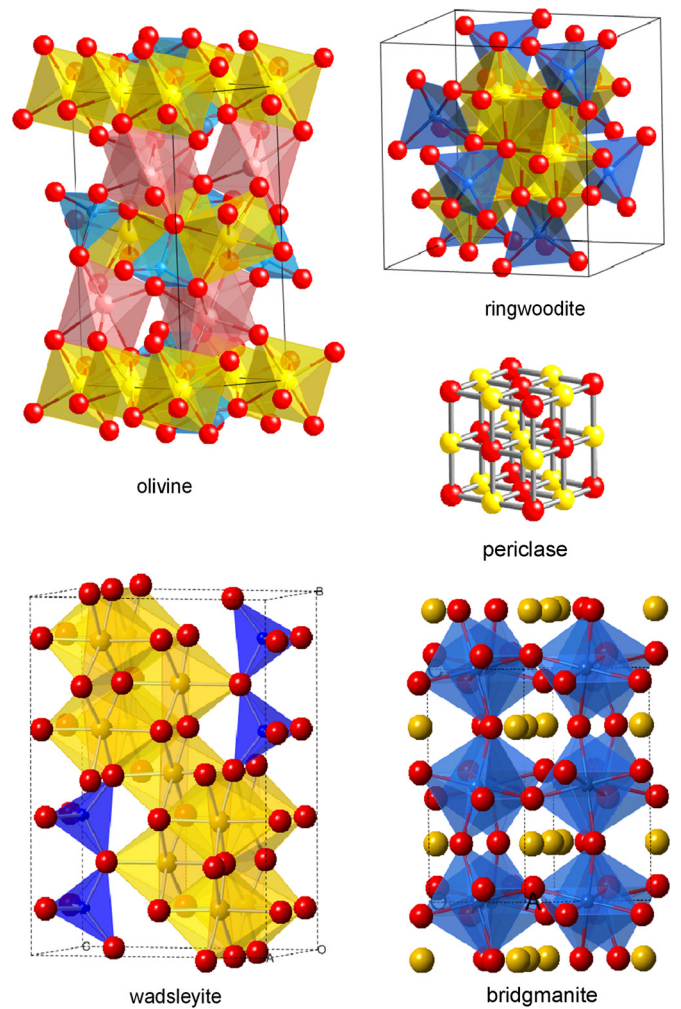

Fig. 1. Crystal structure of olivine and its polymorph. Mg, Si and O are shown in yellow, blue and red, respectively. Si with four nearest neighbor O atoms forms a tetrahedron and Mg with six nearest neighbor O atoms forms an octahedron in forsterite, wadsleyite, and ringwoodite. Si with six nearest neighbor O atoms forms an octahedron in bridgmanite. Mg has 8 nearest neighbor O atoms in bridgmanite. (For interpretation of the references to color in this figure legend, the reader is referred to the web version of this article.)

2000a, 2000b; Li et al., 2007; Wu and Wentzcovitch, 2007; Wu et al., 2008; Yu and Wentzcovitch, 2006). Local density approximation (LDA) for exchange correlation functional (Perdew and Zunger, 1981) is adopted in this study because it has been demonstrated that LDA works well for structures and vibrational properties of minerals. The plane-wave cutoff energy is 70 Ry. Brillouin zone summations over electronic states were performed over $N_1 \times N_2 \times N_3$ k mesh with N_i dependence on the materials (see Table S1). The structures were optimized using variable cell shape molecular dynamics (Wentzcovitch, 1991). Dynamical matrices were computed on regular q mesh using density-functional perturbation theory (DFPT) (Baroni et al., 2001) and then interpolated in a dense q mesh to obtain the vibrational frequencies needed (Table S1).

3. Result: crystal structure and equilibrium isotope fractionation

The crystal lattice parameters of olivine and its polymorphs obtained using first-principles calculations are given in Table 1. The transformation from olivine to wadsleyite and then to ringwoodite does not change the coordination numbers (CN) of Si and Mg atoms (Fig. 1). Si and Mg occupy the tetrahedral and

Table 1
The crystal lattice parameters calculated based on quasi-harmonic approximation from the volume at 0 GPa and 300 K compared with experimental measurements.

	a (Å)	b (Å)	c (Å)	V (Å^3)	
Olivine	4.759	10.200	5.982	290.403	This study
Pnma	4.752	10.192	5.978	289.529	Experiment[a]
	0.2	0.1	0.1	0.3	Error (%)
Wadsleyite	5.7154	11.4591	8.2657	541.35	This study
I4$_1$/a	5.6978	11.4620	8.2572	539.26	Experiment[b]
	0.3	−0.02	0.1	0.4	Error (%)
Ringwoodite	8.079			527.4	This study
	8.076			526.7	Experiment[c]
	0.04			0.1	Error (%)
Periclase	4.219			75.1	This study
	4.212			74.71	Experiment[d]
	0.2			0.5	Error (%)
Bridgmanite	4.7948	4.9458	6.9207	164.1	This study
	4.7782	4.9295	6.8984	162.5	Experiment[e]
	0.3	0.3	0.3	1	Error (%)

Data source for experimental work:
[a] (Kirfel et al., 2005)
[b] (Hazen et al., 2000)
[c] (Meng et al., 1994)
[d] (Dewaele et al., 2000)
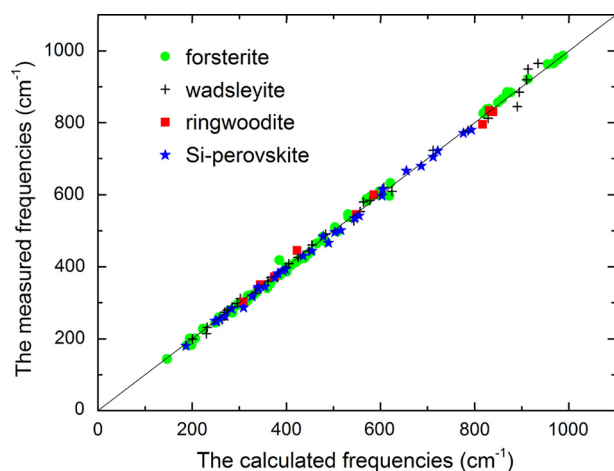[e] (Mao et al., 1991).

Fig. 2. The calculated vibrational frequencies are compared to the measured data (see Table S2 for detail).

octahedral sites, respectively, in all three minerals. In contrast, Si forms octahedra with six O atoms in bridgmanite. Mg CN increases to 8 in bridgmanite. The first-principles calculations with the LDA exchange correlation functional predicted well the crystal structures, vibrational frequency, and thermodynamic properties of olivine and its polymorphs at temperature and pressure conditions of the Earth's mantle (Carrier et al., 2007; Karki et al., 2000a, 2000b; Li et al., 2007; Wu and Wentzcovitch, 2007; Yu and Wentzcovitch, 2006). For example, the calculated lattice constants and vibrational frequencies agree well with experimental data for these minerals (see Tables 1 and S2; Fig. 2). Therefore, LDA is a good exchange correlation functional for isotope fractionation. This has been demonstrated in studies on Mg isotope fractionation between clinopyroxene and pyrope (Huang et al., 2013; Li et al., 2011).

As shown in Fig. 3, the calculated average Mg–O and Si–O bond lengths in several silicate minerals at ambient *P*–*T* conditions agree within ±0.5% (on a relative scale) with the precise XRD measurements. The pressure dependence of the Mg–O and Si–O bond lengths of olivine is consistent with experimental re-
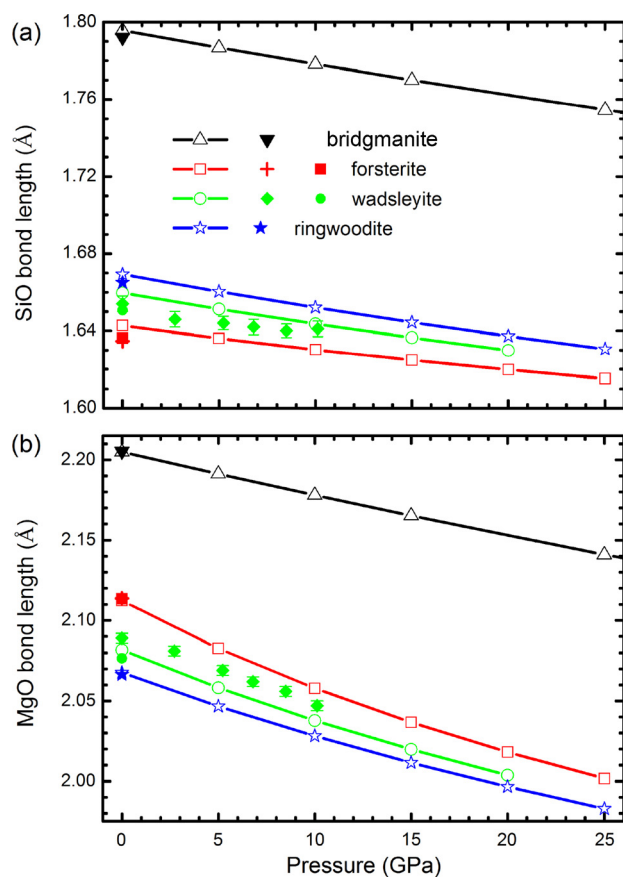

Fig. 3. The pressure dependence of the average bond length for (a) Si–O and (b) Mg–O bond at 300 K. Lines are first-principles calculation results from this study. Experimental data are from Ross and Hazen (1989) (▼), Hazen (1976) (+), Hushur et al. (2009) (■), Hazen (1993) (★), Horiuchi and Sawamoto (1981) (●), Hazen et al. (2000) (◆).

sults. The changes of the Mg–O and Si–O bond lengths are in the opposite directions during transformations from olivine to wadsleyite, then to ringwoodite. The Mg–O bond length decreases during phase transformations in the order of olivine > wadsleyite > ringwoodite, which is consistent with the volume sequence of these phases. In contrast, Si–O bond length increases during these transformations, implying that wadsleyite and ringwoodite have smaller volumes but longer Si–O bond lengths than olivine under the same pressure. Because of the larger Si and Mg CNs in bridgmanite, bridgmanite has much longer Mg–O and Si–O bond lengths than ringwoodite, even though bridgmanite is denser than ringwoodite. The average Mg–O and Si–O bond lengths in bridgmanite are longer than those in ringwoodite at 0 GPa by about 7% and 8%, respectively. Such relative differences increase further with increasing pressure. It is expected that these structure transformations have significant effects on the isotope compositions of Mg and Si of these minerals since they are sensitive to the bond strength and hence bond length.

The calculated reduced partition function ratios ($\ln \beta$) for olivine and its polymorphs at 0 GPa are shown in Fig. 4 and Table 2. ^{26}Mg/^{24}Mg ($10^3 \ln \beta^{Mg}$) decreases in the order of ringwoodite > wadsleyite > ferropericlase > olivine > bridgmanite, while ^{30}Si/^{28}Si ($10^3 \ln \beta^{Si}$) decreases in the order of olivine > wadsleyite > ringwoodite > bridgmanite. These sequences in $10^3 \ln \beta$ are consistent with the sequences of their bond lengths. O isotope fractionations are insensitive to phase transformations from olivine to wadsleyite and then to ringwoodite, because Mg–O bond lengths decrease and Si–O bond lengths increase during these phase transformations and, as a consequence, the average X–O bond lengths
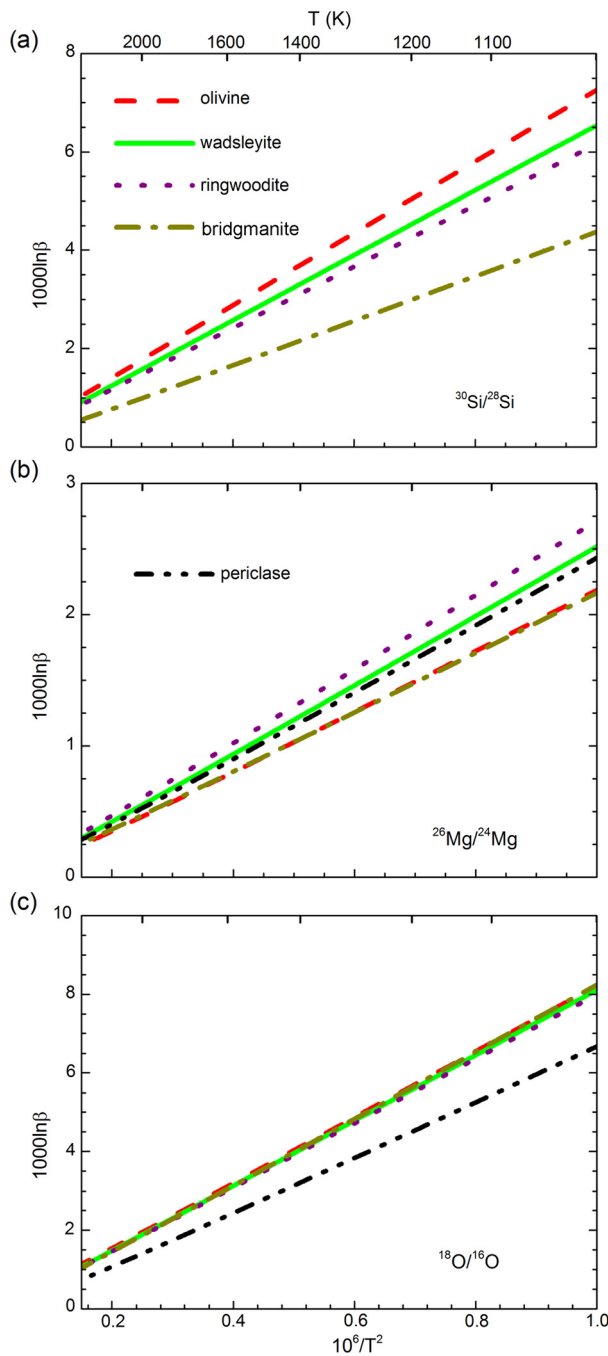
Fig. 4. The temperature dependence of the equilibrium reduced partition function $10^3 \ln \beta$ for (a) ^{30}Si/^{28}Si, (b) ^{26}Mg/^{24}Mg, and (c) ^{18}O/^{16}O of olivine and its polymorphs at 0 GPa.

Table 2
Calculated reduced partition function $1000 \ln \beta$ for olivine, wadsleyite, ringwoodite, bridgmanite, and periclase around 400–3000 K at various pressure.

Pressure			a	b	c
0 GPa	Olivine	Mg	−0.108	2.290	0.0094
		Si	−0.091	7.484	−0.1424
		O	−0.137	8.439	−0.0756
	Wadsleyite	Mg	−0.100	2.615	0.0074
		Si	−0.099	6.741	−0.1067
		O	−0.194	8.386	−0.0754
	Ringwoodite	Mg	−0.093	2.808	0.0049
		Si	−0.097	6.337	−0.0867
		O	−0.187	8.254	−0.0626
	Bridgmanite	Mg	−0.086	2.248	0.0063
		Si	−0.141	4.542	−0.0214
		O	−0.260	8.559	−0.0463
	Periclase	Mg	−0.102	2.526	0.0131
		O	−0.331	7.001	0.0201
13.4 GPa	Olivine	Mg	−0.081	3.112	−0.0042
		Si	−0.053	8.111	−0.1724
		O	−0.143	10.043	−0.1404
	Wadsleyite	Mg	−0.084	3.352	−0.0052
		Si	−0.076	7.454	−0.1393
		O	−0.161	9.828	−0.1219
	Ringwoodite	Mg	−0.083	3.508	−0.0073
		Si	−0.082	7.072	−0.1180
		O	−0.167	9.684	−0.1072
	Bridgmanite	Mg	−0.080	2.710	−0.0008
		Si	−0.121	5.242	−0.0408
		O	−0.228	9.882	−0.0854
	Periclase	Mg	−0.092	3.157	0.0030
		O	−0.293	8.921	−0.0275
23.8 GPa	Olivine	Mg	−0.071	3.685	−0.0149
		Si	−0.041	8.522	−0.1933
		O	−0.096	10.898	−0.1797
	Wadsleyite	Mg	−0.077	3.877	−0.0152
		Si	−0.065	7.949	−0.1632
		O	−0.144	10.851	−0.1571
	Ringwoodite	Mg	−0.077	4.015	−0.0172
		Si	−0.074	7.593	−0.1418
		O	−0.154	10.718	−0.1422
	Bridgmanite	Mg	−0.076	3.056	−0.0066
		Si	−0.109	5.742	−0.0557
		O	−0.209	10.841	−0.1155
	Periclase	Mg	−0.087	3.610	−0.0048
		O	−0.270	10.288	−0.0654

$1000 \ln \beta = a + bx + cx^2$, where $x = 10^6/T^2$. T is temperature in Kelvin.

that ferropericlase has the lowest ^{18}O/^{16}O ($10^3 \ln \beta^O$) among these minerals.

Pressure affects bond strengths and hence $\ln \beta$ (Fig. 5); however, its effect on $\ln \beta$ varies from element to element. Unlike Mg and O, pressure has negligible effect on $10^3 \ln \beta^{Si}$. Pressure effect on $10^3 \ln \beta^O$ is smaller than that on $10^3 \ln \beta^{Mg}$. As shown in Fig. 6, pressure effect on $\ln \beta^{Mg}$ varies from phase to phase. $\ln \beta^{Mg}_{olivine}$ has a stronger pressure dependence than $\ln \beta^{Mg}_{wadsleyite}$ and $\ln \beta^{Mg}_{ringwoodite}$ but weaker than $\ln \beta^{Mg}_{bridgmanite}$. Pressure even changes the sequences of $\ln \beta$. $\ln \beta^{Mg}_{ferroperidase}$ is higher than $\ln \beta^{Mg}_{olivine}$ at 0 GPa but lower than $\ln \beta^{Mg}_{olivine}$ at 24 GPa. Similar pressure effect has been reported by Polyakov (2009) in Fe isotope fractionation between ferropericlase/bridgmanite and metallic Fe, which is negative at 0 GPa but positive at core–mantle boundary. The significant pressure effect on Mg fractionation has also been discussed in other minerals (Huang et al., 2013). These results suggest that pressure is an important factor in determining the equilibrium isotope fractionation for the minerals at the Earth's deep interior, and Mg fractionation between minerals obtained at low pressure may not be applicable to high pressure.

The calculated $\ln \beta$ of olivine's polymorphs along the geotherm (Boehler, 2000) are listed in Tables 3–5, and the differences in

(where X stands for Mg and Si) are similar in these three phases. In addition to bond lengths, the nearest neighbor atoms also affect the isotope fractionations. O isotope fractionation between ringwoodite and bridgmanite is negligible although both Mg–O and Si–O bonds are shorter in ringwoodite than in bridgmanite. O in ringwoodite connects to one Si and three Mg atoms, while O in bridgmanite connects to two Si and two Mg atoms. The Si–O bond is stronger than Mg–O bond in both bridgmanite and ringwoodite, so that bridgmanite and ringwoodite have similar average X–O bond strengths in spite that ringwoodite has a shorter average X–O bond than bridgmanite. The inference that Si–O bond is stronger than Mg–O bond is also consistent with the observation

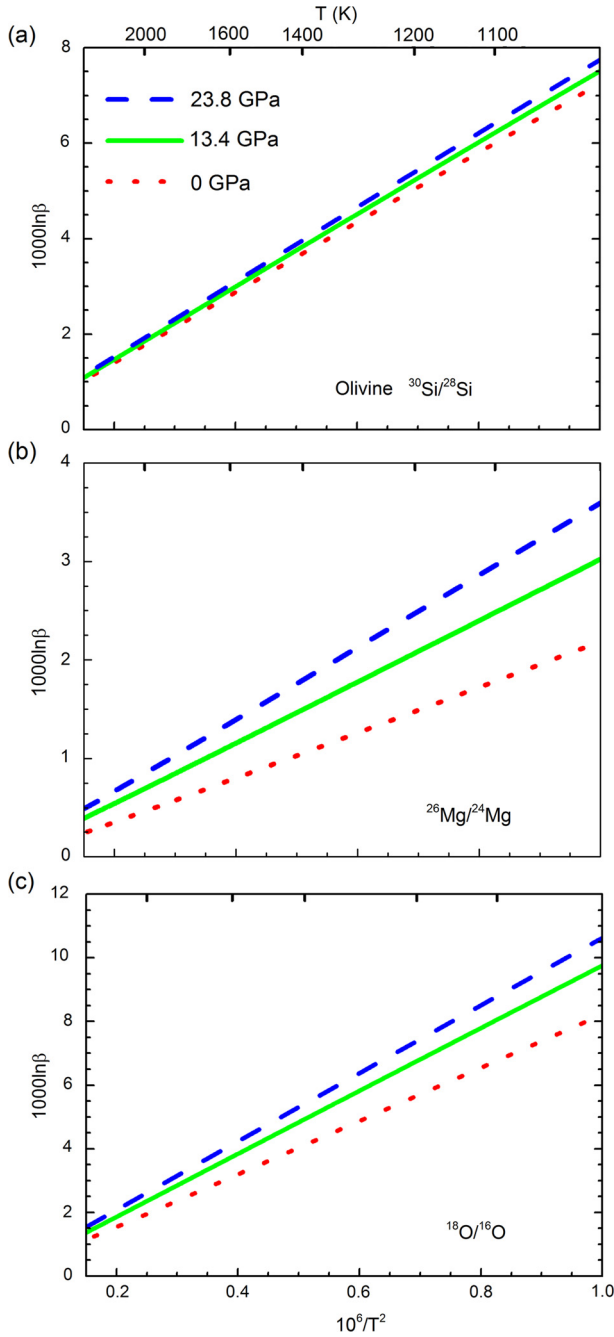**Fig. 5.** The equilibrium reduced partition function $10^3 \ln\beta$ for (a) ^{30}Si/^{28}Si, (b) ^{26}Mg/^{24}Mg, and (c) ^{18}O/^{16}O of olivine at various pressures.

Fig. 6. Temperature dependence of $10^3 \ln\beta_A - 10^3 \ln\beta_B$ for (a) ^{30}Si/^{28}Si, (b) ^{26}Mg/^{24}Mg, and (c) ^{18}O/^{16}O between different minerals (A) and olivine (B) at various pressures.

$10^3 \ln\beta$ at phase boundary along the geotherm are shown in Fig. 7. Mg, Si, and O exhibit different isotope fractionation patterns during the phase transformations. Compared to olivine, wadsleyite and ringwoodite are depleted in ^{30}Si but enriched in ^{26}Mg. Among all phases, bridgmanite shows the largest depletion in both ^{30}Si and ^{26}Mg. Each phase transformation causes measurable isotope fractionations for both Mg and Si isotopes. Si isotope fractionations are larger than Mg isotope fractionations. The significant Si isotope fractionation between bridgmanite and olivine's polymorphs suggests that the Si isotopic fractionation factor between silicate and metal, Δ^{30}Si$_{silicate-metal}$, may decrease with increasing pressure (Georg et al., 2007; Huang et al., 2014). Consequently, Δ^{30}Si$_{silicate-metal}$ obtained from experiments or theoretical calculation at low pressures may not be applicable to Si isotope fraction

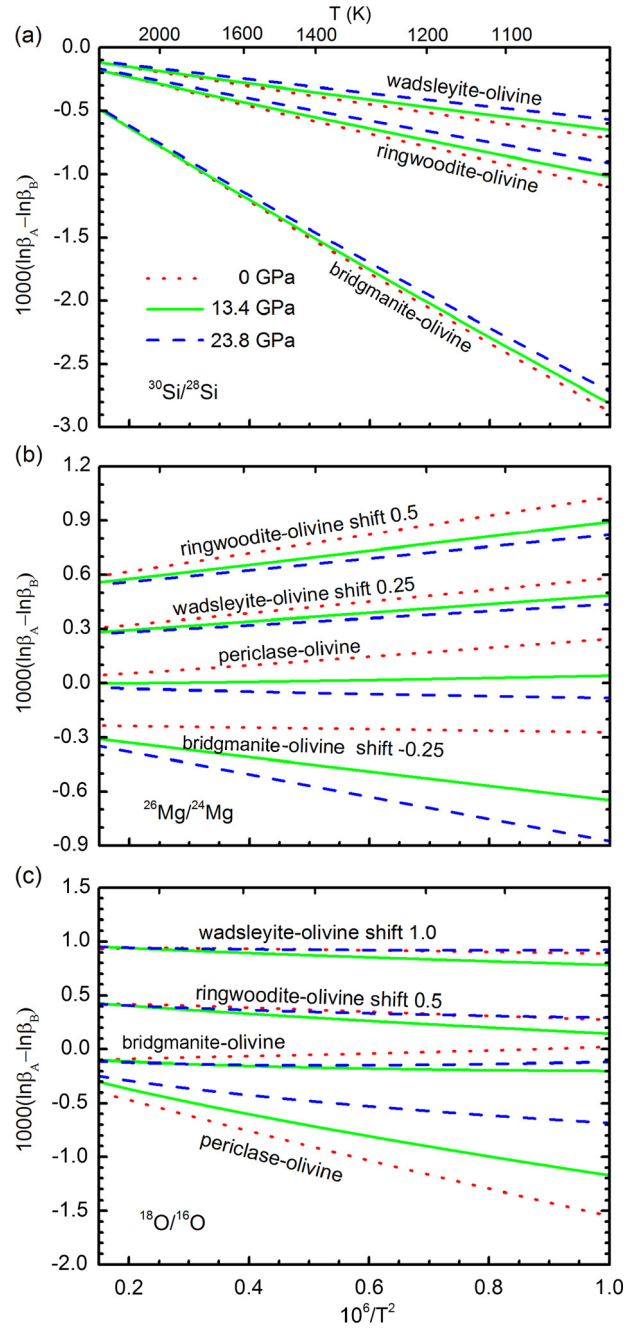during core formation, which may occur at 25–30 GPa (e.g. Li and Agee, 1996; Righter et al., 1997).

4. Implications

Our calculations suggest that the bridgmanite-dominated lower mantle would be slightly enriched in lighter Si and Mg isotopes compared to the olivine-dominated upper mantle during magma ocean cooling process where the upper and lower mantle formed from crystallization of a hot magma ocean (Agee, 1993; Andrault et al., 2011; Rustad and Yin, 2009; Walter et al., 2004). Using the Si CN data of melt from first-principles calculations (Stixrude and Karki, 2005), which show that the average Si CN of melt increases linearly with pressure, and assuming negligible

Table 3
Calculated reduced partition function $1000 \ln \beta$ of $^{30}Si/^{28}Si$ for olivine (Ol), wadsleyite (Wad), ringwoodite (Rin), and bridgmanite (Pv) along geotherm (Boehler, 2000).

P (GPa)	T (K)	Ol	Wad	Rin	Pv
1.70	1388	3.80	3.42	3.21	2.25
1.98	1424	3.62	3.25	3.05	2.13
2.25	1455	3.47	3.12	2.93	2.05
2.58	1482	3.35	3.01	2.83	1.98
3.22	1510	3.25	2.91	2.74	1.92
4.42	1539	3.15	2.83	2.66	1.87
5.74	1566	3.07	2.76	2.60	1.83
7.57	1613	2.93	2.64	2.49	1.76
8.60	1632	2.88	2.60	2.45	1.73
9.51	1651	2.83	2.56	2.41	1.71
10.49	1670	2.78	2.52	2.37	1.69
11.59	1693	2.72	2.47	2.33	1.66
12.35	1707	2.69	2.44	2.31	1.65
13.42	1730	2.64	2.40	2.26	1.62
14.79	1756	2.58	2.35	2.22	1.59
15.77	1777	2.53	2.31	2.18	1.57
16.80	1800	2.48	2.26	2.14	1.54
17.60	1814	2.45	2.24	2.12	1.53
18.50	1830	2.42	2.21	2.10	1.52
19.66	1853	2.37	2.17	2.06	1.49
20.86	1869	2.35	2.15	2.04	1.48
22.04	1881	2.33	2.14	2.03	1.48
23.25	1891	2.32	2.14	2.03	1.48
24.00	1900	2.31	2.13	2.02	1.48
24.50	1904	2.30	2.12	2.02	1.48

Table 5
Calculated reduced partition function $1000 \ln \beta$ of $^{18}O/^{16}O$ for o olivine (Ol), wadsleyite (Wad), ringwoodite (Rin), bridgmanite (Pv) and periclase (Pe) along geotherm (Boehler, 2000).

P (GPa)	T (K)	Ol	Wad	Rin	Pv	Pe
1.70	1388	4.30	4.22	4.16	4.24	3.40
1.98	1424	4.09	4.01	3.95	4.02	3.23
2.25	1455	3.93	3.86	3.80	3.86	3.11
2.58	1482	3.80	3.73	3.67	3.73	3.00
3.22	1510	3.69	3.62	3.56	3.61	2.93
4.42	1539	3.61	3.53	3.48	3.52	2.88
5.74	1566	3.55	3.47	3.41	3.45	2.85
7.57	1613	3.42	3.34	3.28	3.31	2.78
8.60	1632	3.38	3.30	3.24	3.27	2.76
9.51	1651	3.35	3.26	3.21	3.22	2.75
10.49	1670	3.31	3.22	3.17	3.18	2.72
11.59	1693	3.26	3.17	3.12	3.13	2.70
12.35	1707	3.24	3.15	3.09	3.10	2.69
13.42	1730	3.19	3.10	3.05	3.05	2.66
14.79	1756	3.14	3.05	3.00	3.00	2.64
15.77	1777	3.10	3.01	2.96	2.95	2.61
16.80	1800	3.05	2.96	2.91	2.91	2.59
17.60	1814	3.03	2.94	2.89	2.88	2.58
18.50	1830	3.00	2.92	2.87	2.86	2.57
19.66	1853	2.95	2.87	2.83	2.81	2.54
20.86	1869	2.93	2.86	2.81	2.79	2.54
22.04	1881	2.93	2.85	2.81	2.79	2.55
23.25	1891	2.92	2.86	2.81	2.79	2.57
24.00	1900	2.91	2.85	2.80	2.78	2.57
24.50	1904	2.91	2.85	2.81	2.78	2.58

Table 4
Calculated reduced partition function $1000 \ln \beta$ of $^{26}Mg/^{24}Mg$ for olivine (Ol), wadsleyite (Wad), ringwoodite (Rin), bridgmanite (Pv), and periclase (Pe) along geotherm (Boehler, 2000).

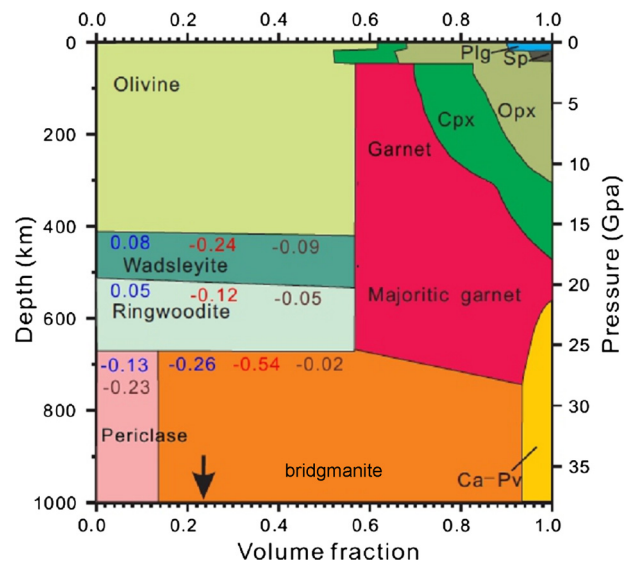| P (GPa)	T (K)	Ol	Wad	Rin	Pv	Pe
1.70	1388	1.13	1.30	1.40	1.10	1.24
1.98	1424	1.08	1.24	1.33	1.05	1.18
2.25	1455	1.04	1.19	1.28	1.01	1.14
2.58	1482	1.01	1.15	1.24	0.97	1.10
3.22	1510	0.99	1.12	1.21	0.94	1.07
4.42	1539	0.98	1.11	1.19	0.92	1.05
5.74	1566	0.98	1.10	1.17	0.91	1.04
7.57	1613	0.97	1.07	1.14	0.88	1.01
8.60	1632	0.97	1.06	1.13	0.87	1.00
9.51	1651	0.97	1.06	1.12	0.86	0.99
10.49	1670	0.96	1.05	1.11	0.85	0.98
11.59	1693	0.96	1.04	1.10	0.84	0.97
12.35	1707	0.96	1.04	1.09	0.83	0.97
13.42	1730	0.95	1.03	1.08	0.82	0.96
14.79	1756	0.95	1.02	1.07	0.81	0.95
15.77	1777	0.94	1.01	1.06	0.80	0.94
16.80	1800	0.94	1.00	1.05	0.79	0.93
17.60	1814	0.94	1.00	1.04	0.78	0.92
18.50	1830	0.94	0.99	1.04	0.78	0.92
19.66	1853	0.93	0.98	1.03	0.77	0.91
20.86	1869	0.93	0.98	1.02	0.77	0.90
22.04	1881	0.94	0.99	1.03	0.77	0.91
23.25	1891	0.95	0.99	1.03	0.77	0.91
24.00	1900	0.95	1.00	1.03	0.77	0.91
24.50	1904	0.95	1.00	1.04	0.77	0.91

Fig. 7. The difference in $10^3 \ln \beta$ caused by phase transformation of Mg_2SiO_4. The value of $10^3 \ln \beta_B - 10^3 \ln \beta_A$ between low-pressure phase A and high-pressure phase B at phase boundary are listed in B phase. Red number is for $^{30}Si/^{28}Si$, blue number is for $^{26}Mg/^{24}Mg$, and wine number is for $^{18}O/^{16}O$. Figure is modified from Frost (2008). (For interpretation of the references to color in this figure legend, the reader is referred to the web version of this article.)

isotope fractionation between melt and minerals with the same CN, we estimated Si isotope fractionation between the lower and upper mantle, $\Delta^{30}Si_{\text{upper mantle–lower mantle}}$, to be 0.08‰ to 0.12‰ (Huang et al., 2014) using mass balance. This fractionation value reflects the upper and lower mantle difference just after the solidification of the magma ocean. This upper and lower mantle Si isotopic difference may still preserve if the primordial lower mantle can be partially preserved or isolated from mantle convection since its formation. As an extreme scenario, if the primordial

lower mantle is completely isolated from the upper mantle, then $\Delta^{30}Si_{\text{upper mantle-bulk silicate earth}} = 0.08‰$, and using the present upper mantle $\delta^{30}Si$ as the bulk silicate earth value would overestimate the Si content in the core by a few weight percent. Specifically, the measured $\delta^{30}Si$ difference between the Earth's upper mantle and the chondritic reservoir ranges from 0.2‰ (Georg et al., 2007) to 0.035‰ (Chakrabarti and Jacobsen, 2010b). Together with a possible 0.08‰ difference between the upper mantle and the bulk silicate Earth inferred from our first-principles calculation, Huang et al. (2014) estimated the Si content in the core at 7.3 wt%

($\Delta^{30}Si_{upper\ mantle–chondritic\ reservoir} = 0.2‰$, Georg et al., 2007) to essentially negligible ($\Delta^{30}Si_{upper\ mantle–chondritic\ reservoir} = 0.035‰$, Chakrabarti and Jacobsen, 2010b).

Equilibrium inter-mineral isotope fractionations have been found in many mantle xenoliths for many elements such as Li, O, Si, Mg, Ca, and Fe (e.g. Chakrabarti and Jacobsen, 2010a; Feng et al., 2014; Georg et al., 2007; Halama et al., 2009; Handler et al., 2009; Huang et al., 2010; Huang et al., 2011; Liu et al., 2011; Savage et al., 2011; Valley et al., 1998; Wiechert and Halliday, 2007; Xiao et al., 2013; Young and Galy, 2004; Young et al., 2002, 2009). Mg isotope fractionation data have been used to constrain the equilibrium temperature of xenoliths based on spinel–olivine pair (Young et al., 2009) and clinopyroxene–garnet pair (Huang et al., 2013). It is also inferred that sizable equilibrium isotope fractionation may also occur even at P–T conditions of the lower mantle (Polyakov, 2009). For example, the equilibrium Fe isotope fractionation during the segregation of Earth's core can explain the enrichment of heavy Fe isotopes in the silicate portions of the Earth and Moon relative to Mars and Vesta (Polyakov, 2009). The significant Si isotope fractionation between bridgmanite and olivine's polymorphs suggests that the lower mantle may have lower $\delta^{30}Si$ than the upper mantle in the early Earth (Huang et al., 2014) as discussed above. Even though the primordial Si isotope heterogeneity between the upper and lower mantle may be destroyed by mantle convection through Earth's history, the inter-mineral isotope fractionation may be preserved due to very slow diffusion in the solid state. Therefore, the olivine in xenoliths that originated from the mantle transition zone or lower mantle may have the isotope compositions expected of olivine's polymorphs or bridgmanite and ferropericlase. Because of this preservation, we suggest that the xenoliths that originated from upper mantle, those from the transition zone, and those from the lower mantle, all may exhibit different Mg and Si equilibrium inter-mineral isotope fractionations. Compared to the xenoliths originating from the upper mantle with equilibrated Mg and Si isotope ratios between olivine and co-existing minerals, the xenoliths that originated from the transition zone or lower mantle may show a seemingly "disequilibrium" Mg and Si isotope fractionation between olivine and co-existing minerals. Specifically, in contrast to the normal olivine, olivine in xenoliths originated from the transition zone will be enriched in ^{26}Mg but depleted in ^{30}Si, while olivine in xenoliths originated from the lower mantle will be depleted in both ^{30}Si and ^{26}Mg. These isotopic patterns are useful in distinguishing the phase transitions from other factors, which can lead to disequilibrium Mg and Si isotope fractionation between olivine and co-existing minerals.

Isotopic diffusion during exhumation and transport to the surface will change the original isotope distribution. Scale of isotope redistribution can be estimated by the diffusion formula, $x^2 = Dt$, where x is the length scale of diffusion and D is the diffusion coefficient. The estimated time t for diffusion across a 1 mm length scale is at the order of 0.15 Ma, using the Mg and Si diffusion coefficient $D \sim 2 \times 10^{-19}$ of $MgSiO_3$ at 25 GPa and 1870 K (Xu et al., 2011). Estimates for the rates of upwelling convective flow and plume flow within the asthenosphere vary from 1 to 100 cm per year (Maclennan et al., 2001) to ~1300 cm per year (Harte and Cayzer, 2007). With an upwelling rate of 100 cm per year, diffusion only modifies the isotope composition of the outermost several mm of the xenolith minerals that were transported to the surface from the transition zone or lower mantle. The interior of the mantle mineral may still keep its original isotopic characteristics at the transition zone or lower mantle. Therefore it is possible that a xenolith that came from the transition zone or lower mantle may still exhibit heterogeneity in Mg, Si, and O isotope reflective of its origin.

Some xenoliths from the island of Malaita in the southwestern Pacific Ocean may come from the mantle transition zone (Collerson et al., 2000) based on their majoritic garnet compositions. One eclogitic xenolith from Oahu, Hawaii has also been suggested as having an origin in the deep upper mantle or the transition zone based on its majoritic garnet composition by Keshav and Sen (2001). If these scenarios are accurate, olivine in these xenoliths may show indicative Mg and Si isotope disequilibrium correlative to our predictions. Studies of inclusions in natural diamonds have indicated that kimberlite eruption can bring diamonds formed in the transition zone or the lower mantle to surface (e.g. Harte, 2010; Kaminsky et al., 2001; Pearson et al., 2014). Some xenoliths and xenocrysts, which erupt together with these diamonds, may also come from the transition zone or lower mantle and hence are also ideal targets to find unusual Mg and Si isotope signatures from the mantle transition zone and lower mantle. If these Mg and Si isotope disequilibrium feature do occur in natural samples, they likely provide additional clues about the original depth of the natural samples and geodynamic process and constraints to temperature in the transition zone or lower mantle.

5. Conclusion

The expected effects of the phase transformations of olivine under pressure on Mg, Si, O isotope fractionations among olivine and its high-pressure polymorphs have been investigated using first-principles calculations. Phase transformations from olivine to wadsleyite, and further to ringwoodite do not change the coordinate number of Mg and Si, yet these phase transformations have measurable and different effects on Mg and Si isotope fractionation. The calculated reduced partition function ratio $\ln \beta$ for $^{26}Mg/^{24}Mg$ decreases in the order of ringwoodite > wadsleyite > olivine, while $\ln \beta$ for $^{30}Si/^{28}Si$ are in the order of olivine > wadsleyite > ringwoodite. This is because during these phase transformations, Mg–O bond length decreases while Si–O bond length increases. Bridgmanite and ferropericlase, which are formed from the dissociation of ringwoodite, have larger Mg and Si coordinate numbers than ringwoodite. Therefore $\ln \beta$ of bridgmanite are significantly smaller than those of ringwoodite for both Si and Mg isotopes. The significant Mg, Si isotope fractionations expected among olivine and its high-pressure polymorphs may provide a way to trace the depth and temperature of origin of xenolith.

Appendix A. Supplementary material

Supplementary material related to this article can be found online at http://dx.doi.org/10.1016/j.epsl.2014.11.004.

References

Agee, C.B., 1993. Petrology of the mantle transition zone. Annu. Rev. Earth Planet. Sci. 21, 19–41.

Albarede, F., Beard, B., 2004. Analytical methods for non-traditional isotopes. Geochem. Non-Tradit. Stable Isotopes 55, 113–152.

Anderson, A.T., Clayton, R.N., Mayeda, T.K., 1971. Oxygen isotope thermometry of mafic igneous rocks. J. Geol. 79, 715.

Andrault, D., Bolfan-Casanova, N., Lo Nigro, G., Bouhifd, M.A., Garbarino, G., Mezouar, M., 2011. Solidus and liquidus profiles of chondritic mantle: implication for melting of the Earth across its history. Earth Planet. Sci. Lett. 304, 251–259.

Baroni, S., de Gironcoli, S., Dal Corso, A., Giannozzi, P., 2001. Phonons and related crystal properties from density-functional perturbation theory. Rev. Mod. Phys. 73, 515–562.

Bigeleisen, J., Mayer, M.G., 1947. Calculation of equilibrium constants for isotopic exchange reactions. J. Chem. Phys. 15, 261–267.

Blanchard, M., Poitrasson, F., Meheut, M., Lazzeri, M., Mauri, F., Balan, E., 2009. Iron isotope fractionation between pyrite (FeS_2), hematite (Fe_2O_3) and siderite ($FeCO_3$): a first-principles density functional theory study. Geochim. Cosmochim. Acta 73, 6565–6578.

Boehler, R., 2000. High-pressure experiments and the phase diagram of lower mantle and core materials. Rev. Geophys. 38, 221–245.

Bourdon, B., Tipper, E.T., Fitoussi, C., Stracke, A., 2010. Chondritic Mg isotope composition of the Earth. Geochim. Cosmochim. Acta 74, 5069–5083.

Carrier, P., Wentzcovitch, R., Tsuchiya, J., 2007. First-principles prediction of crystal structures at high temperatures using the quasiharmonic approximation. Phys. Rev. B 76.

Chakrabarti, R., Jacobsen, S.B., 2010a. The isotopic composition of magnesium in the inner Solar System. Earth Planet. Sci. Lett. 293, 349–358.

Chakrabarti, R., Jacobsen, S.B., 2010b. Silicon isotopes in the inner Solar System: implications for core formation, solar nebular processes and partial melting. Geochim. Cosmochim. Acta 74, 6921–6933.

Clayton, R.N., 1986. High-temperature isotope effects in the early Solar-System. Rev. Miner. 16, 129–140.

Collerson, K.D., Hapugoda, S., Kamber, B.S., Williams, Q., 2000. Rocks from the mantle transition zone: majorite-bearing xenoliths from Malaita, southwest Pacific. Science 288, 1215–1223.

Dewaele, A., Fiquet, G., Andrault, D., Hausermann, D., 2000. $P–V–T$ equation of state of periclase from synchrotron radiation measurements. J. Geophys. Res. 105, 2869–2877.

Emiliani, C., 1955. Pleistocene temperatures. J. Geol. 63, 538–578.

Feng, C., Qin, T., Huang, S., Wu, Z., Huang, F., 2014. First-principles investigations of equilibrium calcium isotope fractionation between clinopyroxene and Ca-doped orthopyroxene. Geochim. Cosmochim. Acta 143, 132–142.

Frost, D.J., 2008. The upper mantle and transition zone. Element 4, 171–176.

Georg, R.B., Halliday, A.N., Schauble, E.A., Reynolds, B.C., 2007. Silicon in the Earth's core. Nature 447, 1102–1106.

Giannozzi, P., Baroni, S., Bonini, N., Calandra, M., Car, R., Cavazzoni, C., Ceresoli, D., Chiarotti, G.L., Cococcioni, M., Dabo, I., Dal Corso, A., de Gironcoli, S., Fabris, S., Fratesi, G., Gebauer, R., Gerstmann, U., Gougoussis, C., Kokalj, A., Lazzeri, M., Martin-Samos, L., Marzari, N., Mauri, F., Mazzarello, R., Paolini, S., Pasquarello, A., Paulatto, L., Sbraccia, C., Scandolo, S., Sclauzero, G., Seitsonen, A.P., Smogunov, A., Umari, P., Wentzcovitch, R.M., 2009. QUANTUM ESPRESSO: a modular and open-source software project for quantum simulations of materials. J. Phys. Condens. Matter 21, 395502.

Halama, R., Savov, I.P., Rudnick, R.L., McDonough, W.F., 2009. Insights into Li and Li isotope cycling and sub-arc metasomatism from veined mantle xenoliths, Kamchatka. Contrib. Mineral. Petrol. 158, 197–222.

Handler, M.R., Baker, J.A., Schiller, M., Bennett, V.C., Yaxley, G.M., 2009. Magnesium stable isotope composition of Earth's upper mantle. Earth Planet. Sci. Lett. 282, 306–313.

Harte, B., 2010. Diamond formation in the deep mantle: the record of mineral inclusions and their distribution in relation to mantle dehydration zones. Mineral. Mag. 74, 189–215.

Harte, B., Cayzer, N., 2007. Decompression and unmixing of crystals included in diamonds from the mantle transition zone. Phys. Chem. Miner. 34, 647–656.

Hazen, R.M., 1976. Effects of temperature and pressure on crystal-structure of forsterite. Am. Mineral. 61, 1280–1293.

Hazen, R.M., 1993. Comparative compressibilities of silicate spinels – anomalous behavior of $(Mg,Fe)_2SiO_4$. Science, vol. 259, pp. 206–209.

Hazen, R.M., Weinberger, M.B., Yang, H.X., Prewitt, C.T., 2000. Comparative high-pressure crystal chemistry of wadsleyite, β-$(Mg_{1-x}Fe_x)_2SiO_4$, with $x = 0$ and 0.25. Am. Mineral. 85, 770–777.

Horiuchi, H., Sawamoto, H., 1981. β-Mg_2SiO_4 – single-crystal X-ray-diffraction study. Am. Mineral. 66, 568–575.

Huang, F., Glessner, J., Ianno, A., Lundstrom, C., Zhang, Z.F., 2009. Magnesium isotopic composition of igneous rock standards measured by MC-ICP-MS. Chem. Geol. 268, 15–23.

Huang, S., Farkas, J., Jacobsen, S.B., 2010. Calcium isotopic fractionation between clinopyroxene and orthopyroxene from mantle peridotites. Earth Planet. Sci. Lett. 292, 337–344.

Huang, F., Zhang, Z.F., Lundstrom, C.C., Zhi, X.C., 2011. Iron and magnesium isotopic compositions of peridotite xenoliths from Eastern China. Geochim. Cosmochim. Acta 75, 3318–3334.

Huang, F., Chen, L.J., Wu, Z., Wang, W., 2013. First-principles calculations of equilibrium Mg isotope fractionations between garnet, clinopyroxene, orthopyroxene, and olivine: implications for Mg isotope thermometry. Earth Planet. Sci. Lett. 367, 61–70.

Huang, F., Wu, Z., Huang, S., Wu, F., 2014. First-principles calculations of equilibrium silicon isotope fractionation among mantle minerals. Geochim. Cosmochim. Acta 140, 509–520.

Hushur, A., Manghnani, M.H., Smyth, J.R., Nestola, F., Frost, D.J., 2009. Crystal chemistry of hydrous forsterite and its vibrational properties up to 41 GPa. Am. Mineral. 94, 751–760.

Ito, E., Takahashi, E., 1989. Postspinel transformations in the system Mg_2SiO_4–Fe_2SiO_4 and some geophysical implications. J. Geophys. Res. B, Solid Earth Planets 94, 10637–10646.

Javoy, M., Balan, E., Meheut, M., Blanchard, M., Lazzeri, M., 2012. First-principles investigation of equilibrium isotopic fractionation of O- and Si-isotopes between refractory solids and gases in the solar nebula. Earth Planet. Sci. Lett. 319, 118–127.

Kaminsky, F.V., Zakharchenko, O.D., Davies, R., Griffin, W.L., Khachatryan-Blinova, G.K., Shiryaev, A.A., 2001. Superdeep diamonds from the Juina area, Mato Grosso State, Brazil. Contrib. Mineral. Petrol. 140, 734–753.

Karki, B.B., Wentzcovitch, R.M., de Gironcoli, S., Baroni, S., 2000a. Ab initio lattice dynamics of $MgSiO_3$ perovskite at high pressure. Phys. Rev. B 62, 14750–14756.

Karki, B.B., Wentzcovitch, R.M., de Gironcoli, S., Baroni, S., 2000b. High-pressure lattice dynamics and thermoelasticity of MgO. Phys. Rev. B 61, 8793–8800.

Katsura, T., Ito, E., 1989. The system Mg_2SiO_4–Fe_2SiO_4 at high-pressures and temperatures – precise determination of stabilities of olivine, modified spinel, and spinel. J. Geophys. Res. B, Solid Earth Planets 94, 15663–15670.

Keshav, S., Sen, G., 2001. Majoritic garnets in Hawaiian xenoliths: preliminary results. Geophys. Res. Lett. 28, 3509–3512.

Kieffer, S.W., 1982. Thermodynamics and lattice-vibrations of minerals. 5. Applications to phase-equilibria, isotopic fractionation, and high-pressure thermodynamic properties. Rev. Geophys. 20, 827–849.

Kirfel, A., Lippmann, T., Blaha, P., Schwarz, K., Cox, D.F., Rosso, K.M., Gibbs, G.V., 2005. Electron density distribution and bond critical point properties for forsterite, Mg_2SiO_4, determined with synchrotron single crystal X-ray diffraction data. Phys. Chem. Miner. 32, 301–313.

Li, J., Agee, C.B., 1996. Geochemistry of mantle–core differentiation at high pressure. Nature 381, 686–689.

Li, X.F., Liu, Y., 2011. Equilibrium Se isotope fractionation parameters: a first-principles study. Earth Planet. Sci. Lett. 304, 113–120.

Li, L., Wentzcovitch, R.M., Weidner, D.J., Da Silva, C.R.S., 2007. Vibrational and thermodynamic properties of forsterite at mantle conditions. J. Geophys. Res. 112, B05206.

Li, X.F., Zhao, H., Tang, M., Liu, Y., 2009. Theoretical prediction for several important equilibrium Ge isotope fractionation factors and geological implications. Earth Planet. Sci. Lett. 287, 1–11.

Li, W.Y., Teng, F.Z., Xiao, Y.L., Huang, J.A., 2011. High-temperature inter-mineral magnesium isotope fractionation in eclogite from the Dabie orogen, China. Earth Planet. Sci. Lett. 304, 224–230.

Liu, L.G., 1976. Post-spinel phase of forsterite. Nature 262, 770–772.

Liu, S.A., Teng, F.Z., Yang, W., Wu, F.Y., 2011. High-temperature inter-mineral magnesium isotope fractionation in mantle xenoliths from the North China craton. Earth Planet. Sci. Lett. 308, 131–140.

Maclennan, J., McKenzie, D., Gronvold, K., 2001. Plume-driven upwelling under central Iceland. Earth Planet. Sci. Lett. 194, 67–82.

Mao, H.K., Hemley, R.J., Fei, Y., Shu, J.F., Chen, L.C., Jephcoat, A.P., Wu, Y., Bassett, W.A., 1991. Effect of pressure, temperature, and composition on lattice-parameters and density of $(Fe,Mg)SiO_3$-perovskites to 30 GPa. J. Geophys. Res. B, Solid Earth Planets 96, 8069–8079.

Meheut, M., Lazzeri, M., Balan, E., Mauri, F., 2007. Equilibrium isotopic fractionation in the kaolinite, quartz, water system: prediction from first-principles density-functional theory. Geochim. Cosmochim. Acta 71, 3170–3181.

Meheut, M., Lazzeri, M., Balan, E., Mauri, F., 2009. Structural control over equilibrium silicon and oxygen isotopic fractionation: a first-principles density-functional theory study. Chem. Geol. 258, 28–37.

Meng, Y., Fei, Y., Weidner, D.J., Gwanmesia, G.D., Hu, J., 1994. Hydrostatic compression of γ-Mg_2SiO_4 to mantle pressures and 700-K – thermal equation of state and related thermoelastic properties. Phys. Chem. Miner. 21, 407–412.

Pearson, D.G., Brenker, F.E., Nestola, F., McNeill, J., Nasdala, L., Hutchison, M.T., Matveev, S., Mather, K., Silversmit, G., Schmitz, S., Vekemans, B., Vincze, L., 2014. Hydrous mantle transition zone indicated by ringwoodite included within diamond. Nature 507, 221.

Perdew, J.P., Zunger, A., 1981. Self-interaction correction to density-functional approximations for many-electron systems. Phys. Rev. B 23, 5048–5079.

Polyakov, V.B., 2009. Equilibrium iron isotope fractionation at core–mantle boundary conditions. Science 323, 912–914.

Righter, K., Drake, M.J., Yaxley, G., 1997. Prediction of siderophile element metal–silicate partition coefficients to 20 GPa and 2800 °C: the effects of pressure, temperature, oxygen fugacity, and silicate and metallic melt compositions. Phys. Earth Planet. Inter. 100, 115–134.

Ringwood, A.E., 1991. Phase-transformations and their bearing on the constitution and dynamics of the mantle. Geochim. Cosmochim. Acta 55, 2083–2110.

Ross, N.L., Hazen, R.M., 1989. Single-crystal X-ray-diffraction study of $MgSiO_3$ perovskite from 77-K to 400-K. Phys. Chem. Miner. 16, 415–420.

Rustad, J.R., Dixon, D.A., 2009. Prediction of iron-isotope fractionation between hematite (α–Fe_2O_3) and ferric and ferrous iron in aqueous solution from density functional theory. J. Phys. Chem. A 113, 12249–12255.

Rustad, J.R., Yin, Q.Z., 2009. Iron isotope fractionation in the Earth's lower mantle. Nat. Geosci. 2, 514–518.

Savage, P.S., Georg, R.B., Williams, H.M., Burton, K.W., Halliday, A.N., 2011. Silicon isotope fractionation during magmatic differentiation. Geochim. Cosmochim. Acta 75, 6124–6139.

Schauble, E.A., 2004. Applying stable isotope fractionation theory to new systems. Geochem. Non-Tradit. Stable Isotopes 55, 65–111.

Schauble, E.A., 2011. First-principles estimates of equilibrium magnesium isotope fractionation in silicate, oxide, carbonate and hexaaquamagnesium (2+) crystals. Geochim. Cosmochim. Acta 75, 844–869.

Stixrude, L., Karki, B., 2005. Structure and freezing of $MgSiO_3$ liquid in Earth's lower mantle. Science 310, 297–299.

Teng, F.Z., Wadhwa, M., Helz, R.T., 2007. Investigation of magnesium isotope fractionation during basalt differentiation: implications for a chondritic composition of the terrestrial mantle. Earth Planet. Sci. Lett. 261, 84–92.

Teng, F.Z., Li, W.Y., Ke, S., Marty, B., Dauphas, N., Huang, S.C., Wu, F.Y., Pourmand, A., 2010. Magnesium isotopic composition of the Earth and chondrites. Geochim. Cosmochim. Acta 74, 4150–4166.

Teng, F.Z., Dauphas, N., Helz, R.T., Gao, S., Huang, S.C., 2011. Diffusion-driven magnesium and iron isotope fractionation in Hawaiian olivine. Earth Planet. Sci. Lett. 308, 317–324.

Tipper, E.T., Galy, A., Bickle, M.J., 2008a. Calcium and magnesium isotope systematics in rivers draining the Himalaya-Tibetan-Plateau region: lithological or fractionation control? Geochim. Cosmochim. Acta 72, 1057–1075.

Tipper, E.T., Louvat, P., Capmas, F., Galy, A., Gaillardet, J., 2008b. Accuracy of stable Mg and Ca isotope data obtained by MC-ICP-MS using the standard addition method. Chem. Geol. 257, 65–75.

Urey, H.C., 1947. The thermodynamic properties of isotopic substances. J. Chem. Soc., 562–581.

Valley, J.W., 1986. Stable isotope geochemistry of metamorphic rocks. Rev. Miner. 16, 445–489.

Valley, J.W., 2001. Stable isotope thermometry at high temperatures. Stable Isotope Geochem. 43, 365–413.

Valley, J.W., Kinny, P.D., Schulze, D.J., Spicuzza, M.J., 1998. Zircon megacrysts from kimberlite: oxygen isotope variability among mantle melts. Contrib. Mineral. Petrol. 133, 1–11.

Walter, M.J., Nakamura, E., Tronnes, R.G., Frost, D.J., 2004. Experimental constraints on crystallization differentiation in a deep magma ocean. Geochim. Cosmochim. Acta 68, 4267–4284.

Wang, S.J., Teng, F.Z., Williams, H.M., Li, S.G., 2012. Magnesium isotopic variations in cratonic eclogites: origins and implications. Earth Planet. Sci. Lett. 359, 219–226.

Wentzcovitch, R.M., 1991. Invariant molecular-dynamics approach to structural phase-transitions. Phys. Rev. B 44, 2358–2361.

Wentzcovitch, R.M., Yu, Y.G.G., Wu, Z.Q., 2010. Thermodynamic properties and phase relations in mantle minerals investigated by first principles quasiharmonic theory. Rev. Mineral. Geochem. 71, 59–98.

Wiechert, U., Halliday, A.N., 2007. Non-chondritic magnesium and the origins of the inner terrestrial planets. Earth Planet. Sci. Lett. 256, 360–371.

Wu, Z., Wentzcovitch, R.M., 2007. Vibrational and thermodynamic properties of wadsleyite: a density functional study. J. Geophys. Res. 112, B12202.

Wu, Z., 2010. Calculating the anharmonic free energy from first principles. Phys. Rev. B 81, 172301.

Wu, Z., Wentzcovitch, R.M., 2011. Quasiharmonic thermal elasticity of crystals: an analytical approach. Phys. Rev. B 83.

Wu, Z., Wentzcovitch, R.M., Umemoto, K., Li, B.S., Hirose, K., Zheng, J.C., 2008. Pressure–volume–temperature relations in MgO: an ultrahigh pressure–temperature scale for planetary sciences applications. J. Geophys. Res. 113, B06204.

Xiao, Y., Teng, F.Z., Zhang, H.F., Yang, W., 2013. Large magnesium isotope fractionation in peridotite xenoliths from eastern North China craton: product of melt-rock interaction. Geochim. Cosmochim. Acta 115, 241–261.

Xu, J.S., Yamazaki, D., Katsura, T., Wu, X.P., Remmert, P., Yurimoto, H., Chakraborty, S., 2011. Silicon and magnesium diffusion in a single crystal of $MgSiO_3$ perovskite. J. Geophys. Res. 116.

Young, E.D., Galy, A., 2004. The isotope geochemistry and cosmochemistry of magnesium. Geochem. Non-Tradit. Stable Isotopes 55, 197–230.

Young, E.D., Ash, R.D., Galy, A., Belshaw, N.S., 2002. Mg isotope heterogeneity in the Allende meteorite measured by UV laser ablation-MC-ICPMS and comparisons with O isotopes. Geochim. Cosmochim. Acta 66, 683–698.

Young, E.D., Tonui, E., Manning, C.E., Schauble, E., Macris, C.A., 2009. Spinel-olivine magnesium isotope thermometry in the mantle and implications for the Mg isotopic composition of Earth. Earth Planet. Sci. Lett. 288, 524–533.

Yu, Y.G.G., Wentzcovitch, R.M., 2006. Density functional study of vibrational and thermodynamic properties of ringwoodite. J. Geophys. Res. 111, B12202.

Yu, Y.G.G., Wu, Z., Wentzcovitch, R.M., 2008. α–β–γ transformations in Mg_2SiO_4 in Earth's transition zone. Earth Planet. Sci. Lett. 273, 115–122.

Zheng, Y.F., Fu, B., Gong, B., Li, L., 2003. Stable isotope geochemistry of ultrahigh pressure metamorphic rocks from the Dabie–Sulu orogen in China: implications for geodynamics and fluid regime. Earth-Sci. Rev. 62, 105–161.